

# Structural and optical properties of nanostructured tungsten trioxide thin films prepared by aqueous chemical growth

B T Sone<sup>1,2</sup>, C Nlagamandla<sup>1</sup>, T. Malwela<sup>3</sup>, R Bucher<sup>1</sup>, E Iwuoha<sup>2</sup> and M Maaza<sup>1</sup>

<sup>1</sup>NANOAFNET-Africa Nanocentre, Materials Research Department, iThemba LABS, P.O. Box 722, Somerset West, 7129, South Africa.

<sup>2</sup>Chemistry Department, University of the Western Cape, Bellville, South Africa.

<sup>3</sup>National Centre for Nanostructured Materials, CSIR, P.O. Box 395, Pretoria, South Africa.

Email: sonebert@tlabs.ac.za, sonebert@gmail.com

**Abstract.** Crystalline thin solid films of WO<sub>3</sub> have been prepared on Corning glass and FTO through the low temperature, wet chemistry method of Aqueous Chemical Growth. SEM images of the thin films produced show that the surface morphology of the films is influenced by the kind of substrate used for the synthesis. While nanoplatelet-containing flower-like structures were consistently obtained on the Corning glass substrates, nanorod-containing urchin-like structures were consistently produced on the F-doped SnO<sub>2</sub>-glass substrates. Structural characterization of the different thin films synthesized on both substrates was carried out using XRD, TEM, HRTEM and SAED. These showed that the films produced were made up of WO<sub>3</sub> in the monoclinic, cubic and hexagonal phase depending on what heat-treatment procedures the different substrates were subjected to post-synthesis. The quantum confinement effect is clearly demonstrated in the thin films on Corning glass as the optical band gap calculated for these films was seen to undergo a blue shift from the theoretical values of 2.7eV in the bulk to values of 3.18eV, 3.93eV, and 4.12eV at the nano/microscale.

## 1. Introduction

WO<sub>3</sub> is a wide band gap, 2.7eV, n-type semiconductor metal oxide (SMO) [1,8] that has been widely investigated for its gas sensing, electrochromic, gasochromic and catalytic properties[1,2,8]. It finds applications in a wide variety of devices which include among others optical switching devices, optical data storage devices, smart windows and gas sensors [1,2, 5].

WO<sub>3</sub> is more widely used in the form of thin films and coatings than bulk and has been prepared in this form using both physical and chemical methods which include pulsed laser deposition, electron beam evaporation, radio frequency magnetron sputtering, electrospinning, spray pyrolysis, thermal evaporation, chemical vapour deposition, sol-gel chemistry, hydrothermal synthesis[5,8]. The physical deposition techniques are generally energy intensive, costly, not easily scaled-up, are known to lead to the formation of amorphous films and coatings, but are more tunable in terms of determining film and surface coating thickness. The soft chemistry techniques are known to be less costly, less energy intensive, result in crystalline thin films but are less tunable in terms of determining film thickness. We have recently used,

for the first time, the soft-chemistry technique of Aqueous Chemical Growth (ACG) [3,4 ] to prepare, at low temperature (95°C), WO<sub>3</sub> thin films on Corning Glass (CG) and F-doped SnO<sub>2</sub>-Glass (FTO) substrates. ACG is a low temperature, soft-chemistry, environmentally benign technique that offers the possibility of building well-ordered, highly crystalline metal oxide thin films over a wide variety of substrates with large array, by using metal salts of desired metal oxides in aqueous media [3,4]. By varying pH, concentration and time of synthesis, it is possible to influence the structure of the films produced.

## 2. Experimental

Pale yellow acidic solutions of Peroxotungstic acid (PTA), iso-propanol and de-ionised water with  $0.2 < \text{pH} < 2.5$  were prepared through slight modification of a method used in [5] for the synthesis of electrospun WO<sub>3</sub>-PVP nanofibres on aluminium. Corning glass and FTO substrates (1 mm thick), cleaned by sequential ultrasonication in solutions of MeOH, acetone and de-ionised water for periods of 5 min each, then dried with N<sub>2</sub>, were then placed at an angle 70° to the horizontal, in Schott® bottles containing the acidified mixture. These were then tightly sealed and placed in a pre-heated (90-95°C) laboratory oven for 6-24h. The as-synthesized thin films grown on both substrates were generally greenish-yellow in color or whitish. Once removed, these were washed and dried in air after which calcination in air at 500°C, for 1-2h, rendered them yellowish-green and strongly adhered to the substrate surface.

The morphology of the thin films' surfaces, the structures therein and chemical analysis of the surfaces was determined using Scanning Electron Microscopy (SEM) measurements performed on a LEO-Stereo Scan 440 Scanning Electron Microscope coupled to a unit for Electron Dispersive X-Ray Spectroscopy (EDX). Crystal structure was ascertained by X-Ray Diffraction (XRD) on a BRUKER AXS D8 Advance X-Ray Diffractometer equipped with a Cu K $\alpha$  monochromator, at wavelength,  $\lambda = 1.540315$  nm. To ascertain the morphology as well as the crystallinity of the structures produced Transmission Electron Microscopy (TEM) was carried out on Field Emission Gun-TEM with an accelerating voltage of 200kV, while High Resolution TEM (HRTEM) and Selected Area Electron Diffraction (SAED) were carried out on a TECNAI F20 FEG-TEM. Absorption and Transmission spectra of WO<sub>3</sub> thin films were measured in the UV-Visible-Near IR range (200-1100 nm) using a CECIL 2000 Spectrophotometer with the incident beam at the normal to the substrates.

## 3. Results & Discussions

### 3.1. Surface Morphology by Scanning Electron Microscopy and Chemical analysis by EDX

SEM revealed that for ACG carried out on Corning glass substrates, nanoplatelet structures were consistently and primarily formed with thicknesses in the 80-250 nm range and widths/diameters in the 1-2 $\mu$ m range. Also observed in figure 1(a) were nanorods/nanobelts 30-50 nm thick and tens of microns long. In some of the thin films, as in that grown at pH = 0.23 (figure 1(a)), the nanoplatelets assembled to form hierarchically ordered super structures bearing resemblance to desert roses. In other thin films, as in that grown at pH = 0.44, 0.91 (figure 1(b) and (c)), the nanoplatelets were observed to be vertically oriented away from the surface of the glass substrate. On the other hand for ACG carried out on FTO, urchin-like microspheres (figure 2(a) and (b)) were regularly formed as opposed to nanoplatelets. These urchin-like microspherical structures consisted of a sphere-like central core, several microns thick, covered with hair-like protrusions with dimensions in the nanorange. EDX (figures 1(d) and 2(c)) carried out on both samples showed that the films consisted mainly of W and Oxygen. An evaluation of the atomic % of both atoms suggests that WO<sub>3</sub> on the ACG samples in CG is in the 1:4 ratio. This suggests the possibility of the formation of oxygen vacancies in the WO<sub>3</sub> lattice particularly after annealing in air at 500°C. EDX on the FTO-based samples (figure 2(c)) shows alongside W and O, the presence of Sn which

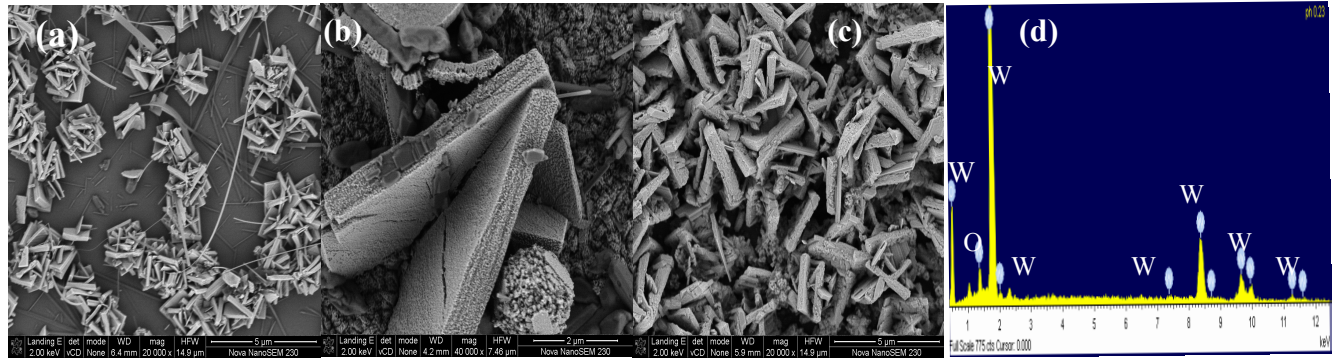


Figure 1. SEM of  $\text{WO}_3$  on Corning glass prepared at (a) pH=0.23; (b) pH=0.44; (c) pH=0.91; (d) EDX spectrum of  $\text{WO}_3$  on CG.

must come from the F-SnO<sub>2</sub> layer. We believe that the morphology of the films produced on FTO is influenced by the crystalline nature of the F-doped SnO<sub>2</sub> layer. As a result of the influence of the crystalline SnO<sub>2</sub> substrate the lattice parameters for  $\text{WO}_3$  thin films on FTO may not be consistent with that of the bulk phase[6].

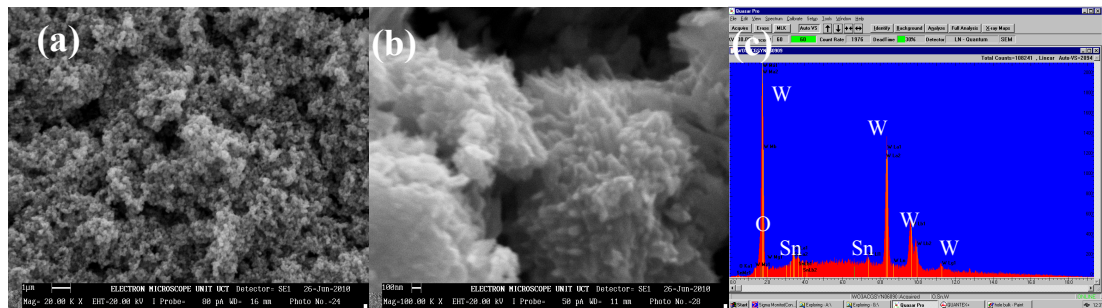


Figure 2 (a) and (b). SEM micrograph of  $\text{WO}_3$  thin film on FTO; (c)  $\text{WO}_3$  EDX spectrum of  $\text{WO}_3$  on FTO.

### 3.2. Crystal structure determination by X-Ray Diffraction (XRD), TEM, HRTEM and SAED

XRD analysis of the  $\text{WO}_3$ -ACG samples on CG and FTO showed  $\text{WO}_3$  the thin films to be in the monoclinic, cubic, and hexagonal phases. Peaks of  $\text{WO}_3$  in the hexagonal phase, figure 3(b), could be indexed to JCPDS Card No. 033-1387 and had reflections of high intensity in the (100), (001), (110), (111) (201), (220), (202), (400), (401) planes. The height and narrowness of the peaks suggest that the  $\text{WO}_3$  thin film, pH = 0.91, was highly crystalline.  $\text{WO}_3$  in this thin film was in the cubic phase and could be indexed to the JCPDS Card No. 041-0905 with reflections in the (100), (110) planes and preferred orientation in the (100) plane. Using the Debye-Scherrer formula the grain size of the  $\text{WO}_3$  thin film, pH = 0.23 was estimated to be ~ 8nm while that of the thin films at pH = 0.44 and 0.91 was estimated to be 17nm.

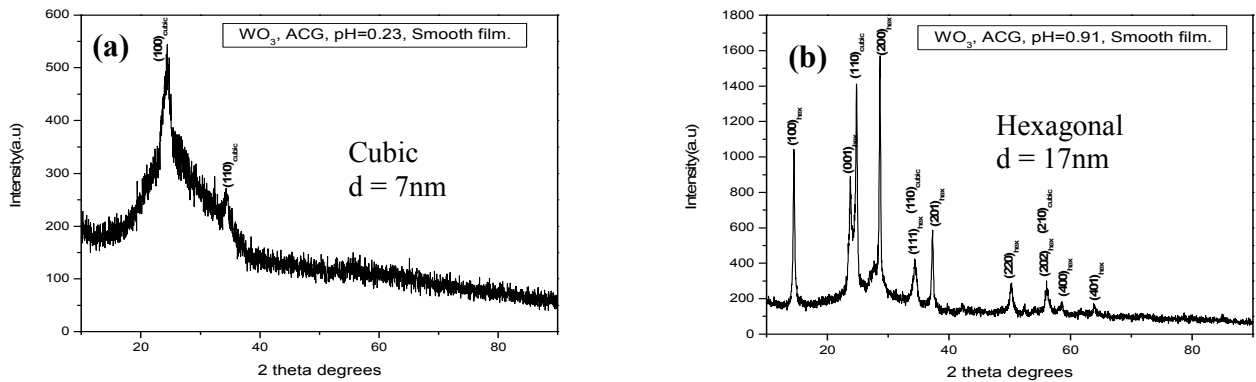


Figure 3. (a) XRD of  $\text{WO}_3$  on C. glass at pH=0.23, pH = 0.91; (b). XRD of  $\text{WO}_3$ -ACG on FTO

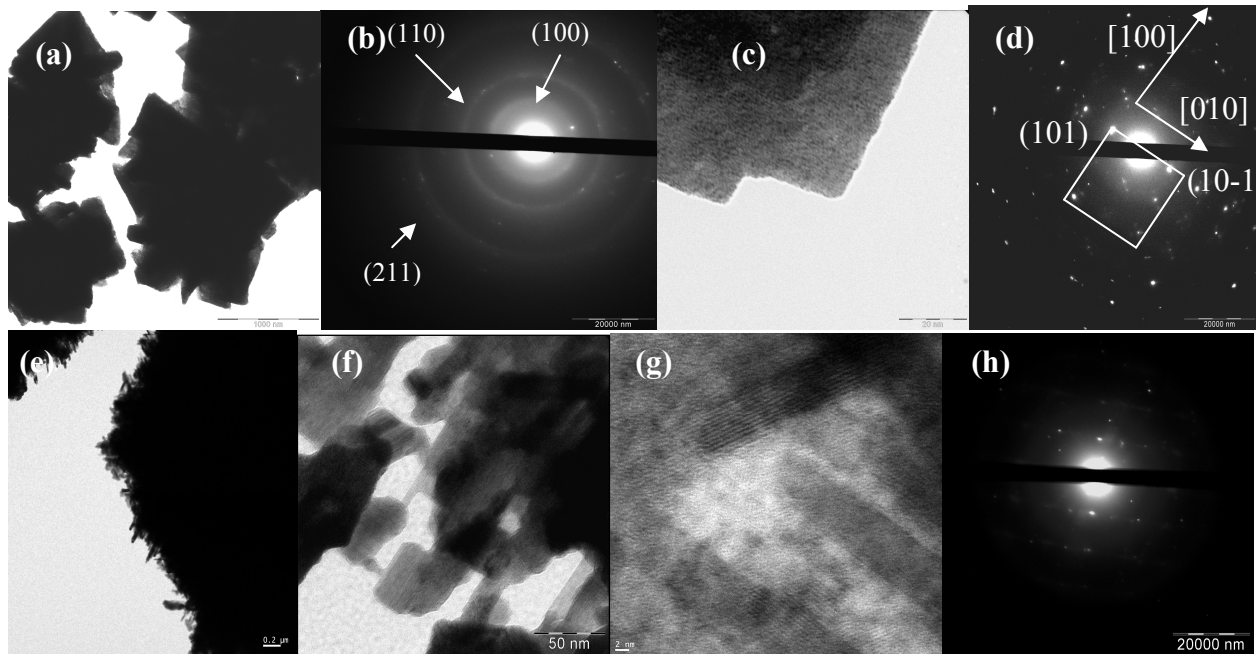


Figure 4. (a) TEM image of  $\text{WO}_3$  nanoplatelets on CG; (b) SAED for  $\text{WO}_3$  nanoplatelets on CG showing the poly- crystalline nature of film; (c) Higher magnification of  $\text{WO}_3$  nanoplatelets on CG; (d) SAED of single crystal  $\text{WO}_3$  nanoplatelets on CG; (e) TEM of  $\text{WO}_3$  microsphere on FTO; (f). TEM of nanorods grown on  $\text{WO}_3$  microsphere; (g) HRTEM nanorods on microsphere; (h) SAED on single crystal of  $\text{WO}_3$  nanorod on microsphere.

TEM (figure 4(a) and 4(c)) carried out on the  $\text{WO}_3$  thin film on Glass, pH = 0.23, showed the nanoplatelet-like structures. SAED (figure 4(b)) on an agglomeration of nanoplatelets showed through the existence of concentric rings that could be indexed to the (100), (110) and (211) planes of  $\text{WO}_3$  of the cubic phase, the polycrystalline nature of the films. SAED (figure 4(d)) showed diffraction spots emanating from a single crystal of the  $\text{WO}_3$  nanoplatelets in the cubic phase; alignment in of the planes in the [100] and [010] direction was clearly visible. Reflections from the (100) and the (110) could be

indexed. TEM (figure 4(e)) on WO<sub>3</sub> urchin-like microspheres showed the thick nature of the spheres, impermeable to the electron beam. The hair-like nanorods were however thin enough to be imaged using TEM (figure 4(f)) and HRTEM (figure 4(g)), from which the lattice fringes in the nano-rod like structures could be observed and was calculated to be 2.52 nm - a value which corresponds to the interplanar spacing  $d_{(202)}$  in monoclinic phase of WO<sub>3</sub> grown on FTO. WO<sub>3</sub> grown on FTO was polymorphic showing the existence of WO<sub>3</sub> in both the monoclinic and hexagonal phase (XRD not shown here), this possibly as a result of the heating that took place at 400°C for 0.5-1h, allowing for the transition in part of WO<sub>3</sub> in the monoclinic phase to WO<sub>3</sub> in the hexagonal phase [6]. Note the two different directions of growth in the HRTEM micrograph of the hair like structures in WO<sub>3</sub> on FTO. SAED on one of the nanorods (figure 4(h)) shows the diffraction spots from a single crystal of the WO<sub>3</sub> hair-like nanorod. Note the streaking in the diffraction patterns which may be attributed to the existence of planar defects and domains within the hair-like protrusions[6].

### 3.4. Optical properties of WO<sub>3</sub> thin films on Corning Glass prepared by ACG

The WO<sub>3</sub> samples on CG and FTO were evaluated for their optical properties in the UV-VIS-NIR region. Film thickness determined using FIB-SEM was estimated at 2 μm for the thin film on CG and 3 μm for the film on FTO. The cut-off wavelength for the thin films on CG produced at pH = 0.23, 0.44, 0.91, lay at the edge of the UV-Visible boundary, 320, 420 and 334 nm respectively. By using the Tauc's relation for indirect semiconductors (equation (1)), (absorption coefficient\* $h\nu$ )<sup>1/2</sup> vs  $h\nu$  (photon energy) was plotted; where  $\alpha$  = absorption coefficient;  $A$  is a constant associated to fundamental band-band transitions constant in the optical frequency range;  $h\nu$  = energy of the incident photons and  $E_g$  = optical band gap or electronic band gap.

$$(ah\nu) = A(h\nu - E_g)^{1/2} \quad (1)$$

$$\alpha = 1/d[\ln(1/T)] \quad (2)$$

$E_g$  which corresponds to indirect transition of photons/electrons between the valence and the conduction band in WO<sub>3</sub> was obtained by extrapolating the linear plot of the curve near the onset of

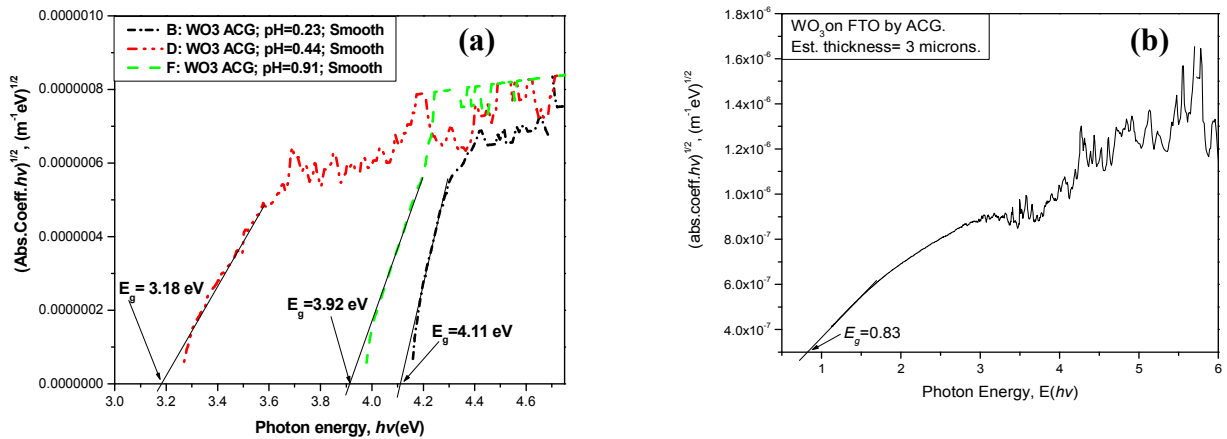


Figure 5. (a) Optical band gap calculation of WO<sub>3</sub> on CG; (b) Optical band gap for WO<sub>3</sub> thin film on FTO.

the absorption edge so that it touched the x-axis at the point where  $(\alpha hv)^{1/2} = 0$ . The absorption coefficient,  $\alpha$ , of the film was calculated using the relation in equation (2), where  $d$  is the thickness of the film as estimated by SEM and  $T$  is the % transmittance of the film.  $E_g$  for the thin film, prepared at pH = 0.44, with thickness 4 $\mu$ m, was calculated to be 3.18eV (see figure 4(a)) while for the thin films prepared at pH =0.23 and 0.91, the optical band gap was calculated to be 4.11 eV and 3.92 eV respectively. The strong linear relationship between  $(\alpha hv)^{1/2}$  and photon energy of the incident light,  $E_g = hv$ , shows that WO<sub>3</sub> is an indirect band gap material. The blue shift observed in the optical band gap can be explained as being a result of the quantum confinement effect that takes place when the size of bulk WO<sub>3</sub> is reduced to the nanoscale. The optical band gap for the WO<sub>3</sub> thin film on FTO (figure 5b) is calculated to be  $E_g = 0.83$  based on UV-Vis-NIR transmission spectrum not shown here. The thin films of WO<sub>3</sub> on Corning glass with their array of closely packed, their reduced grain size in the nanoscale, their vertically oriented nanoplatelets and hierarchical desert rose-like nanostructures should alongside the dense but disordered distribution of microspheres on FTO, offer large surface areas with high porosity that offer increased pathways for gas diffusion making them applicable in gas sensing, electrochromic devices and possibly catalysis [6,7]. The thin films on FTO can be employed as electrochromic material in optical switching devices and smart windows.

#### 4. Conclusion

ACG was used to prepare WO<sub>3</sub> thin films on Corning glass and FTO. SEM and TEM confirm the formation of nanoplatelet and urchin-like structures of WO<sub>3</sub> on the respective substrates. XRD, HRTEM and SAED showed that WO<sub>3</sub> existed in the cubic, hexagonal and monoclinic phase within the films. Average crystallite size for WO<sub>3</sub> in the films on CG was as small as 8 nm. This is less than the Bohr radius of WO<sub>3</sub> and may explaining in part the blue shift in  $E_g$  from 2.7eV in the bulk to 3.18eV, 3.92 eV, 4.11 eV in the WO<sub>3</sub> thin film on CG prepared at pH=0.44, 0.91 and 0.23 respectively. The other factors that may influence the final value for the optical band gap of the films is the film thickness as well as reflectance from the films which was not taken into consideration when calculating the absorption coefficients.

#### Acknowledgements

The financial support of iThemba LABS and Nanoscience Africa Network (NANOAFNET) is hereby acknowledged.

#### References

- [1] Chaudhari G N, Bende A M, Bodade A B, Patil S S, Sapkal V S 2006 *Sensors and Actuators B* **115** 297-302
- [2] Deepa M, Srivastava A K, Sharma S N, Govind and Shivaprasad S M 2008 *Applied Surface Science* **254** 2342-2352
- [3] Vayssieres L, Hagfeldt A, and Lindquist S E 2000 *Pure Applied Chemistry* **72** 47-52
- [4] Lionel Vayssieres 2004 *International Journal of Nanotechnology* **1** No.1/2 1-41
- [5] Xiaofeng L, Xincal L, Zhang W, Wang C., Wei Y 2006 *Journal of Colloid and Interface Science* **298** 996-999
- [6] LeGore L J, Lad R J, Moulzolf S C, Vetelino J F, Frederick B G, Kenik E A 2009 *Thin Solid films* **406** 79-86
- [7] Solis J L, Sauko S, Kish L, Granqvist C G, Lantto V 2001 *Thin Solid Films* **391** 255-360
- [8] Xie G, Yu J, Chen X, Jiang Y 2007 *Sensors and Actuators B* **123** 909-914